U-shaped micropores induced dielectric and piezoelectric tunability in bismuth sodium titanate-based ceramics

Tong Lu[1], Huiling Du[1,*] , Nan Kong[1], Haodong Li[1], Shiyu Xu[1], Zhao Li[1], and Xian Du[1]

[1] College of Materials Science and Engineering, Xi'an University of Science and Technology, Xi'an 710054, Shaanxi, China

ABSTRACT

$Bi_{0.5}Na_{0.5}TiO_3$ (abbreviated as BNT)-based ceramics are considered the promising candidates for lead-free piezoelectric materials to replace the widely used lead zirconate titanate (PZT)-based piezoelectric ceramics. Piezoelectric properties could be modulated by porous structures to meet the needs of piezoelectric energy converters. Porous $(Bi_{0.5}Na_{0.5})_{0.94}Ba_{0.06}TiO_3$ (BNT-6BT) ceramics had been prepared by using kiwi pollen as a sacrificial template for inducing U-shaped micropores. Porosity correlations of dielectric and piezoelectric properties of the porous BNT-6BT ceramics in the relative porosity range of 0–50% were obtained and analyzed. The temperature stability of the dielectric constant of porous ceramics is significantly improved, while the dielectric constant of porous ceramics decreases rapidly with the increase of the amount of pollen added, and then remains stable. The longitudinal piezoelectric coefficient d_{33} and the transverse piezoelectric coefficient d_{31} of porous ceramics decrease slowly with porosity. It was found that the ceramic barrier hinders the pinning effect of the micro stress and strain on domain walls, which makes the piezoelectric properties of porous ceramics well maintained. Porous BNT-based ceramics have great application value in underwater acoustic transducers and other fields.

1 Introduction

Due to their good mechanical properties and stable piezoelectric properties, piezoelectric ceramics are multifunctional materials with a broad range of applications in multiple technological fields such as sensors, ultrasonic transducers, micro displacement devices, and other electronic components [1–3]. PZT-based ferroelectric materials are widely used in resonators, transducers, and memories due to their excellent dielectric properties [4]. With the increasing attention to environmental protection, researchers have been committed to the development of high-performance lead-free piezoelectric ceramics and

found some oxide ceramics with excellent properties, which are expected to replace lead-based ceramics [5].

BNT-based ceramics are a type of important perovskite lead-free ferroelectric and piezoelectric materials [6, 7], which have attracted extensive attention. Structurally, Bi^{3+} and Na^+ occupy the A-site of BNT and are distributed in disorder. BNT-based ceramics are multifunctional materials with a wide range of applications in multiple technical fields, due to their large residual polarization, large electro-induced strain, and typical relaxation properties [8]. However, it has drawbacks such as high coercive field, E_c = 73 kV/cm, and relatively high conductivity. In order to improve the electromechanical coupling performance of BNT ceramics, a lot of research has been done on the morphotropic phase boundary of BNT ceramics in recent years. Among them, BNT-6BT ceramics is a kind of piezoelectric ceramics with deep research because of its high piezoelectric constant (d_{33}) and large strain. Further improving the piezoelectric response of BNT-6BT is of great significance to the development of lead-free piezoelectric materials.

In recent years, the research and application of lead-free porous piezoelectric ceramics have gradually become a hot spot [9–11]. The existence of porosity, especially in some specific configurations, might be beneficial to adjust the functional characteristics in some cases. Porous piezoelectric ceramics not only have a large surface area and lightweight but also have high porosity which simplifies piezoelectric resonance response, maintaining or even increasing tunability [12–14], improving energy conversion efficiency [15, 16]. Exemplary cases also include improving the optimal value of pyroelectricity [17, 18], increasing the hydrostatic pressure optimum value of piezoelectrics, improving the acoustic impedance matching between ceramics and measuring media in underwater sonar or ultrasonic medical imaging [19, 20], reducing the dielectric constant, or changing the characteristics of ferroelectric switches [21–23]. Among various types of porous ceramics, sodium bismuth titanate-based materials have been less studied and have not been considered until recently [23, 24], mainly because they are environment-friendly alternatives to lead-based piezoelectrics. The preparation process of porous ceramics mainly includes (1) partial sintering method; (2) sacrificial template method; (3) copy template method; (4) direct foaming method; (5) 3D printing method [25], in the case (2), a proper amount of pore-forming agents are mixed with ceramic powder and then evaporated or burned out before or during sintering, pores may be created inside the ceramic body that duplicates its size, shape, and distribution. Templates are generally divided into natural organic matter (resin, pollen, cotton, etc.) [26–28], synthetic organic matter (polymer microspheres, organic fibers, etc.) [29, 30], metal and inorganic substances (nickel, fly ash, glass particles, etc.) [31, 32], liquid (water, gel, emulsion, etc.), etc. Commonly used templates are starch, pollen, organic fibers, graphite, and charcoal [33–36]. Kiwi pollen is first selected as a sacrificial template to construct porous ceramics to explore the influence of pore structure on the properties of piezoelectric materials. On the one hand, kiwi pollen has a special structure, on the other hand, it is prolific in the northwestern region of China.

In this study, porous BNT-6BT ceramics with light quality and good performance were obtained by controlling the amount of kiwi pollen added to change the pore number, size and profile of U-shaped micropores. It provides a basis for the further development of piezoelectric energy conversion devices.

2 Experimental procedure

The BNT-6BT powders were prepared by solid-state reaction that used Na_2CO_3 (> 99.8%), Bi_2O_3 (> 99.9%), TiO_2 (> 99.9%), and $BaCO_3$ (> 99.9%) as base materials. The raw materials were weighted according to the nominal stoichiometric ratio and then ball milled for 8 h at 350 r/min with zirconia balls in a nylon bottle with 20 mL ethanol. The obtained solution was then dried for 12 h. The dried powders were calcined at 870 °C for 3 h and then re-milled for 6 h to break agglomerates. After drying, the powders passed through 100 mesh sieve.

Porous BNT-6BT ceramics were prepared by sacrificial template method. The template selected in this experiment is kiwi pollen (Meixian County, Baoji, Shaanxi). In order to ensure that the pollen structure is not broken, the dry mixing method was selected to mix the ceramic powder and pollen directly and evenly. Put the ceramic powder into the mold and press it as a green body with a diameter of about 10 mm and a thickness of about 1 mm, and place the

ceramic green body in a vacuum bag for isostatic pressing to complete the preparation of the ceramic sample. All porous ceramic samples were heated at 3 °C/min to 550 °C for 2 h to burn the pollen template. Finally, porous BNT-6BT ceramics were obtained by sintering at 1100–1120 °C for 2 h. As a reference, dense ceramics are produced under the same conditions without adding any sacrificial templates. Silver was fabricated onto the surface of the ceramic and heated at 800 °C for 15 min at a heating rate of 5 °C/min.

In this experiment, X-ray diffractometer (D8 advance, AXS company in Brooke, Germany) was used to check the purity and structural phase composition of the sample. The target used was copper target, and $K_{\alpha 1} = 1.5406$. The scanning angle was from 10 to 80°, with a step length of 0.2°, a scan speed of 5°/min, a step width of 0.02, a voltage of 36 kV, and a current of 20 mA. The morphology of ceramics was examined by high-resolution scanning electron microscope (FE-SEM; S-4800, Hitachi, Japan), and the total pore volume, pore size distribution and porosity were measured by mercury intrusion method using mercury porosimeter (Anton Parconta PoreMaster 60). The dielectric constant, dielectric loss and dielectric frequency/temperature characteristics of the samples were measured by precision LCR analyzer Agilent E4980A and GJW-I high temperature dielectric temperature spectrum test system (Institute of electronic materials, Xi'an Jiaotong University). The longitudinal piezoelectric coefficient d_{33} of all ceramic samples were measured at 110 Hz using DZ-2671A withstand voltage tester and ZJ-5A quasi-static piezoelectric constant tester.

3 Results and discussion

X-ray diffraction patterns of porous BNT-6BT ceramics with different pollen additions are shown in Fig. 1a. They all show the presence of perovskite structure. It can be seen from the local enlarged drawing (Fig. 1b) that the strongest diffraction peaks of porous ceramics shift to lower angles. For porous ceramics in this paper, the crystal structure and diffraction peaks are affected by the grain structure and pore structure. After the sacrificial template is treated at a high temperature, the porous structure is induced, resulting in changes in the internal stress of the ceramic [37, 38]. As sintering progresses, the amount of pollen gradually decreases, the grains gradually grow, the pore size shrinks, and tensile stresses are generated between the grains on the pore wall and the grains inside the ceramic. The tensile stress causes the micro displacement of the crystal cell, resulting in the cell parameters becoming larger, and thus the maximum diffraction peak shifts to a lower angle.

The biological template kiwi pollen was used as pore-forming agent to prepare porous BNT-6BT ceramics. Figure 1c shows the SEM micrographs of the kiwi pollen. Kiwi pollen grains from Baoji, Shaanxi province, containing particles with regular size (average diameter of 20–50 μm), ellipsoid or superlong sphere, with concave inclusions. The main reason for choosing kiwi pollen as pore-forming agent is that it has a certain aspect ratio morphology structure. For piezoelectric ceramics, previous researchers found that larger aspect ratio can significantly increase the longitudinal piezoelectric coefficient [39, 40]. As shown in Fig. 1d, BNT-6BT powder is spherical and similar in size (average size ∼ 300 nm).

In the following, porous BNT-6BT samples will be expressed as 0%, 2.5%, 5%, 10%, 12.5% and 15% respectively according to their pollen addition. Figure 2 shows the surface morphology of porous ceramics. From the figure, it can be seen that there are U-shaped microporous in the sample. As the firing process proceeds, the pollen template induced the same pore as the pollen structure. The ceramic protrusions offer barriers in the U-shaped micropores, which divide the pores into two interconnected regions. When the amount of pollen added is 5 wt%, the corresponding relative porosity is 15.8%, and the number of pores is small. The profile of the pore is ellipsoidal, and the aspect ratio is approximately 2:1, which corresponds to the pollen microstructures of Fig. 1c. The SEM micrographs show that with the increasing amount of pollen added, the number of pores increased gradually, and the porosity increased from 5 to 43.6%. The pore size is gradually increased, probably due to the pollen agglomeration, which causes the continuous stacking of pollen grains to make the pore channels larger and rounder. In the dense regions, the grain size is in the range of about 1.5 μm for the 5% ceramic and decreases down to about ∼ 1 μm when adding pollen template, for all the porosities.
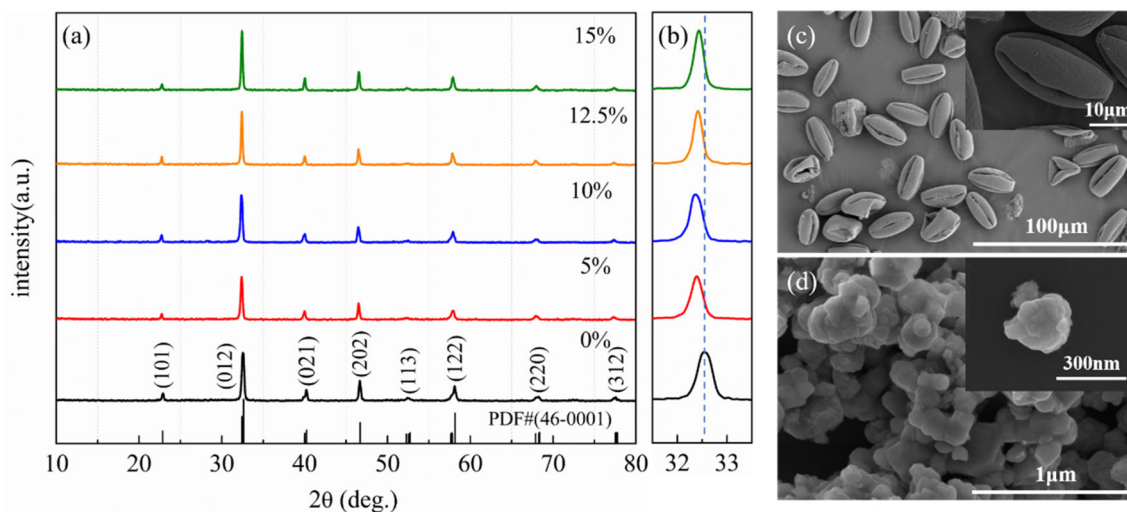
Fig. 1 a X-ray diffraction patterns of porous BNT-6BT ceramics with different pollen additions. **b** XRD patterns of 32–33°. **c** SEM micrographs of the kiwi pollen **d** SEM micrographs of BNT-6BT powders

The relationship between porosity and relative permittivity of porous piezoelectric ceramics can be predicted. Figure 3a shows the porosity and relative permittivity experimental values of porous BNT-6BT ceramics compared to the predicted values at a 1 kHz test frequency. This is due to the decreasing ceramic phase and the increasing air phase, where the dielectric constant is much lower than that of the ceramic phase. The cube correction model proposed by Banno [41] is used for the prediction. The calculation results are similar to the experimental measurement results, and they are widely accepted. The calculation formula is as follows:

$$\varepsilon_{33p} = \varepsilon_{33d}\left[1 + \frac{1}{p^{1/3}(\varepsilon_{33d}/\varepsilon_0 - 1)K_s^{2/3} + 1} \times \frac{p^{2/3}}{K_s^{2/3}} - \frac{p^{2/3}}{K_s^{2/3}}\right]$$
(1)

where, ε_{33p} is the dielectric constant of porous piezoelectric ceramics; ε_{33d} is the dielectric constant of dense piezoelectric ceramics; p is the porosity; K_s is the shape factor (spherical hole: $K_s=1$, oval hole: $K_s=0.5$). Due to the large dielectric constant of compact ceramics, Eq. 2 can be simplified as follows:

$$\varepsilon_{33p} = \varepsilon_{33d}\left[1 - \frac{p^{2/3}}{K_s^{2/3}}\right]$$
(2)

From Fig. 3a, the relative permittivity ε_r of BNT-6BT porous ceramics is distributed between a shape factor (K_s) of 0.5 and 1. By adjusting the K_s, the

experimental data match well with the theoretical values. When the porosity is less than 10%, the distribution of the relative permittivity ε_r is highly consistent with the curve of $K_s=0.5$, when the pore profile is mainly ellipsoid. When the porosity is greater than 10%, the test value of the relative permittivity ε_r is more consistent with the curve of $K_s=0.7$, which is due to the increase of porosity and the pore profile gradually becomes spherical, as evidenced by the micromorphology Fig. 3b and c maps of BNT-6BT porous ceramics.

Figure 4a–e shows the temperature change curves of the dielectric constant (ε_r) and the dielectric loss (tanδ) in the porous BNT-6BT ceramic samples with different pollen additions. All the samples exhibit distinct relaxation features, with two dielectric anomalous diffusion peaks appearing in the test temperature range. The dielectric constant ε_{max} maintains above 1500. The temperature (T_m) corresponding to ε_{max} is 280 °C. In perovskite structures, when multiple ions jointly occupy a certain lattice position, these ion distributions are disordered, causing uneven chemical composition and crystal structure at the microscopic scale. Under the action of the AC electric field, these different microregions (polar microregions or microdomains) have different frequency responses, leading to different polarization behavior, and then polarization relaxation occurs [42]. For BNT-6BT ceramic material system, its A position is occupied by Na$^+$, Bi^{3+}, and Ba^{2+} ions, which inevitably leads to the inhomogeneity of
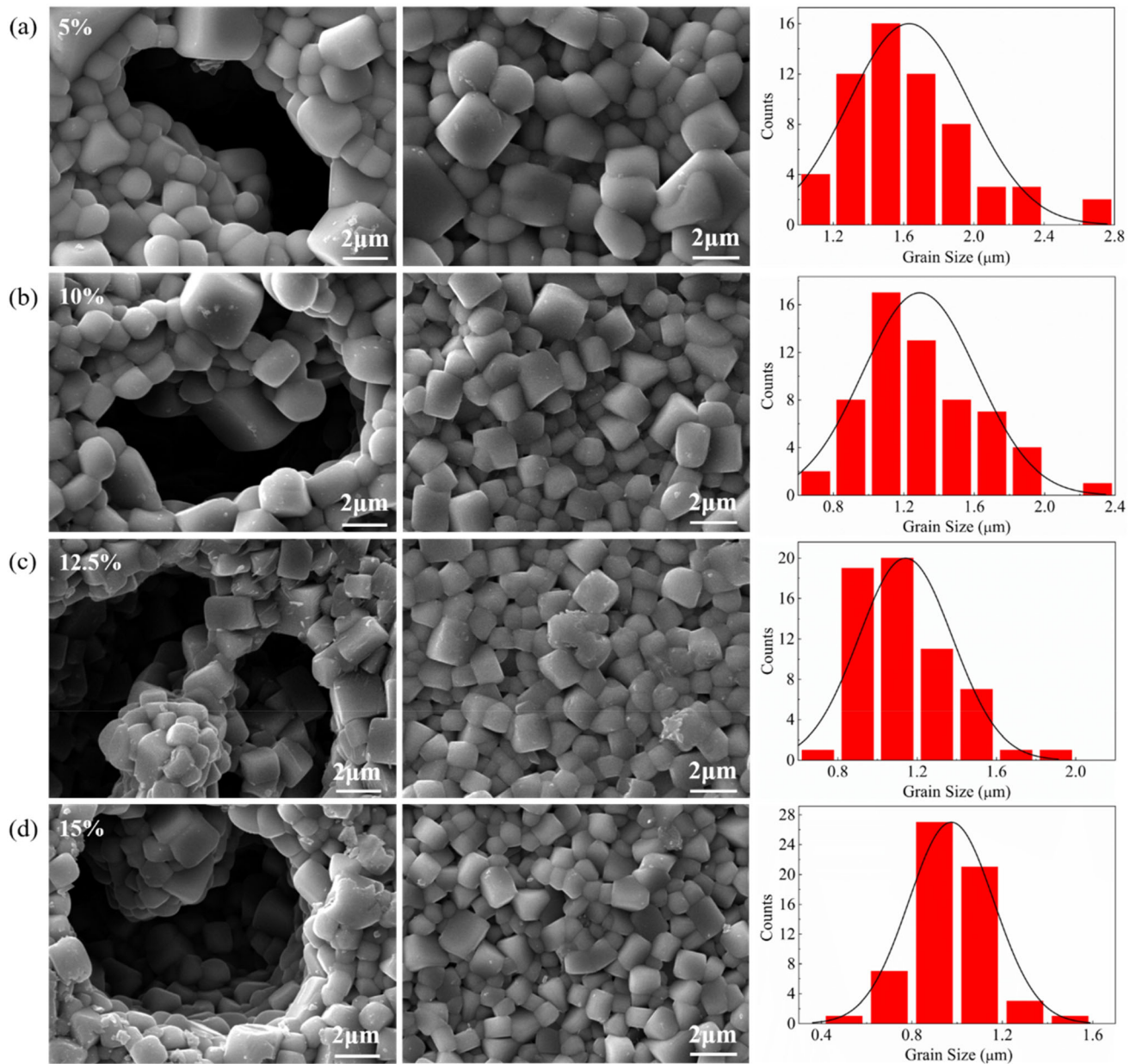
Fig. 2 the surface morphology of porous ceramics prepared with pollen as pore forming agent **a** 5%, **b** 10%, **c** 12.5%, **d** 15%

nanoscale chemical composition and crystal structure, and further leads to ferroelectric relaxation. The dielectric loss of porous BNT-6BT ceramics decreases rapidly with the increase in temperature, possibly because the lattice distortion decreases with the increase of temperature, which makes domain turning easier and the relaxation polarization loss smaller. Before T_m, the dielectric loss of dense ceramics was higher than that of porous ceramics because in the presence of pores, the air pore interface acts as a pinning center for domain walls, which evolve under heterogeneous fields, reducing their mobility and the losses associated with domain walls [37]. When the temperature exceeds the T_m, dielectric loss increases with temperature rise rapidly. The reason may be that when heated to a certain temperature, the conductive mechanism of piezoelectric ceramics gradually changes from ionic conductivity to electronic conductivity. The leakage current loss of samples increases rapidly, and the resistivity of ceramics decreases sharply, which makes the dielectric loss of porous BNT-6BT ceramics increase rapidly.
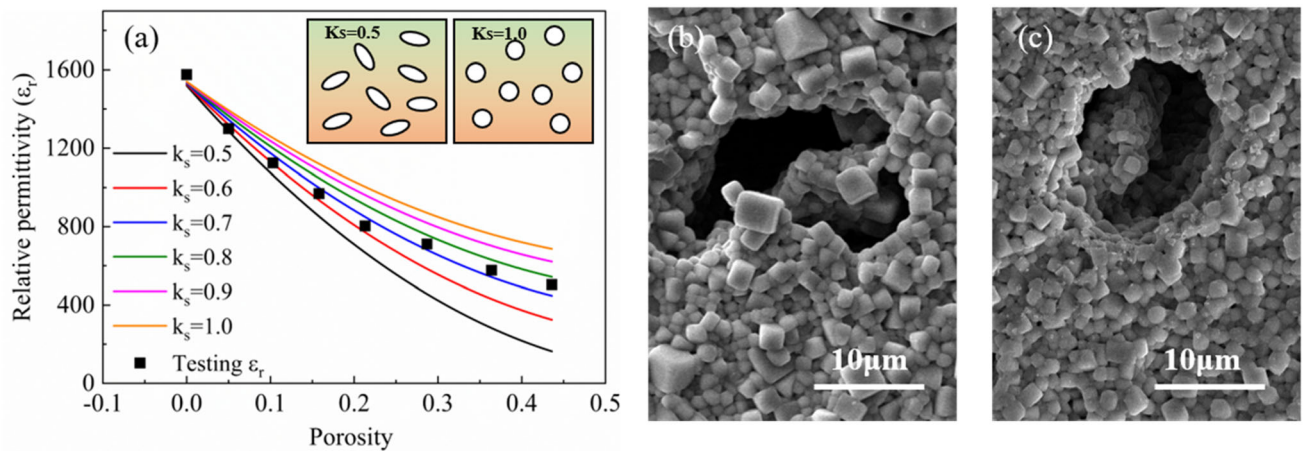
Fig. 3 **a** Comparison between experimental values and predicted values of Banno model. **b** SEM diagram of ceramic sample with 5% pollen addition **c** SEM diagram of ceramic sample with 15% pollen addition
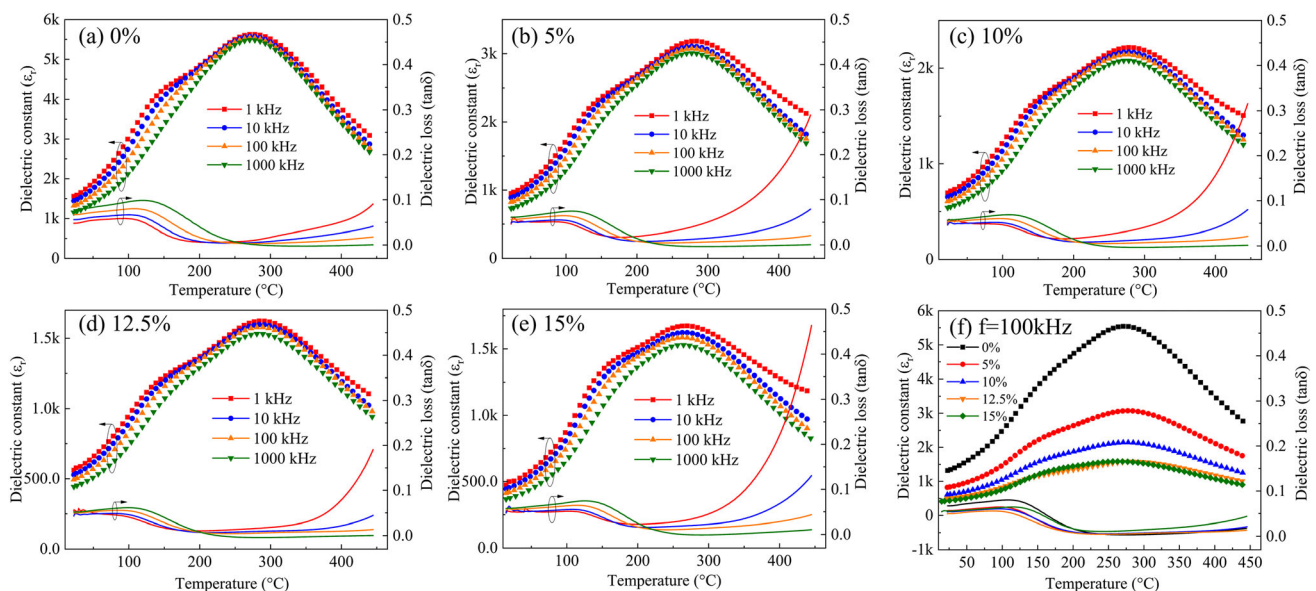

Fig. 4 Temperature dependence of dielectric constant and dielectric loss of porous BNT-6BT ceramics

Figure 4f is the curve of the dielectric constant and dielectric loss with the temperature of the ceramic sample at 1 kHz. The addition of pollen leads to a significant reduction in the dielectric constant of the material, and with the increase in the amount of pollen adds, the dielectric constant continues to decrease. When the amount of pollen is more than 12.5%, the dielectric constant gradually remains stable. Compared with compact ceramics, the dielectric constant of porous BNT-6BT ceramics varies less with the temperature, and the thermal stability of the dielectric constant is significantly improved.

The aperture distribution of porous ceramics is shown in Fig. 5a. The pores in the ceramic samples are mainly distributed between 5 and 20 μm. Unimodal pore size distribution was observed in 5% ceramics, and with the increase of pollen addition, the pore size distribution changed from unimodal to bimodal. Because when the amount of pollen is large, the continuous stacking of pollen particles makes the pore channels larger and rounder, and the pore size distribution gradually becomes bimodal. The pore size gradually increased, and the peak intensity increased, indicating that the porous ceramic sample was mainly composed of pores with larger pore sizes.
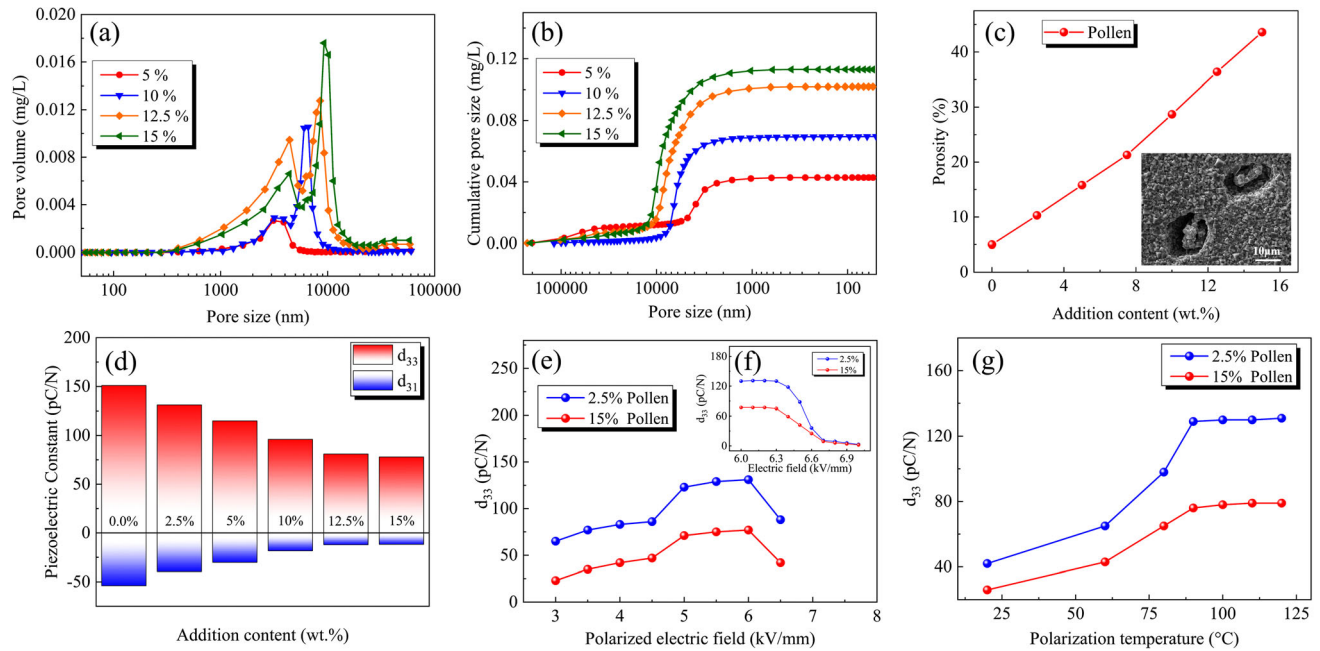
Fig. 5 a Pore size distribution. **b** Cumulative pore volume distribution. **c** Relationship between porosity and pollen added amount. **d** Relationship between pollen addition and d_{33} and d_{31}. **e** Relationship between polarization temperature and d_{33}. **f** Variation trend of d_{33} under polarized electric field intensity of 6–7 kV/mm. **g** Relationship between polarized electric field and d_{33}

The average pore size of 5% ceramics is much smaller than the size of pollen because as the sintering progresses, the pollen gradually decreases, the grains gradually grow, and the pore size shrinks. The average pore size of 5% ceramics is much smaller than that observed by SEM, which is due to the small amount of pollen added, pollen particles are more dispersed in the sample, and there are closed pores in the sintered ceramic sample. Only open pores were tested when measuring pore size distribution, resulting in an average pore size of 5% ceramics much smaller than the size of pollen and the pore size observed by SEM. The cumulative pore distribution results of different porous ceramic samples are shown in Fig. 5b. The cumulative pore volume distribution curves for all samples exhibit different platform heights when the pollen addition increased from 5 to 15 wt%. The height of the platform represents the porosity of the sample. With the increase of the amount of pollen added, the porosity gradually increases. The relationship between pollen addition and porosity is shown in Fig. 5c. By using different amounts of pollen addition, porosity from 5% (corresponding to the reference sample without pore-forming agent) to 43.6% is produced, and the porosity

has a quasi-linear relationship with the amount of pollen addition. After sintering, the samples perfectly duplicate the morphology of pollen and form pores in the ceramics.

After polarization, the anisotropic ferroelectric domain deflects along the direction of the electric field, and still retains a certain degree of orientation after the polarization electric field is removed, thus showing piezoelectricity. The more sufficient the polarization is, the higher the measured longitudinal piezoelectric coefficient d_{33} is. Figure 5d is the relationship curve between the amount of pollen added and the longitudinal piezoelectric coefficient d_{33} of porous BNT-6BT ceramics. It can be seen from the figure that the longitudinal piezoelectric coefficient d_{33} of porous BNT-6BT ceramics gradually decreases with the increase of pollen content. On the one hand, as the amount of the pore phase increases, the piezoelectric phase content of the porous ceramics decreases, thus resulting in the decrease of the longitudinal piezoelectric coefficient d_{33}. On the other hand, d_{33} reflects the change of potential shift under stress or the change of strain under an electric field. The potential shift and strain are related to the polarization of materials and the migration of domain

walls. For porous piezoelectric ceramics, the internal stress around the pore causes micro-stress and strain. With the increase of porosity, the pinning effect of micro-stress and strain on the domain wall increases gradually, which hinders the polarization of the material and reduces the piezoelectric coefficient of the material [43]. The porous ceramics prepared with pollen as a sacrificial template show good piezoelectric performance, with a porosity of 10.3% at 2.5% pollen addition and d_{33} of 131pC/N, and only a 13.2% reduction in d_{33} compared to dense ceramics. Because the pollen has a special structure, U-shaped micropores are formed inside the ceramic after sintering. According to the stress concentration model and the stress theory of Carroll and Holt [44], the internal stresses present around the pores leading to the microscopic stress and strain of the porous BNT-6BT ceramics. However, the ceramic barrier inhibits the concentration of micro stress around the micropores, hinders the pinning effect of micro stress and strain on the domain wall, and makes the piezoelectric constant better maintained. In Fig. 5d, the variation trend of transverse piezoelectric coefficient d_{31} is the same as that of longitudinal piezoelectric coefficient d_{33}. With the increase in pollen content, the transverse piezoelectric coefficient d_{31} decreases.

Porous BNT-6BT ceramics were polarized by changing the intensity of polarization electric field under the conditions of polarization time of 30 min, pressure holding for 15 min and polarization temperature of 90 °C. Porous ceramics with pollen additions of 2.5 and 15 wt% were studied as representatives. The variation law of longitudinal piezoelectric coefficient d_{33} (measured at 110 Hz) with polarization electric field intensity E is shown in Fig. 5e. When $E < 4.5$ kV/mm, d_{33} increases slowly with the increase of E. At this stage, only the easy-turning electric domains can be deflected along the direction of the external electric field. When $E > 4.5$ kV/mm, the external electric field is greater than the coercivity field of the material, d_{33} increases rapidly with the increase of E. When $E > 6$ kV/mm, the local temperature of the crystal rises due to the increase in current, resulting in local melting and structural destruction of the crystal, so that the piezoelectric performance of the ceramic decreases until it breaks. Figure 5f shows the variation trend of d_{33} of porous ceramics under the polarization electric field intensity of 6–7 kV/mm. When $E = 6.2$ kV/mm, the value of d_{33} reaches the maximum, and then

gradually decreases until the ceramic sheet is broken down. Thus, $E = 6$ kV/mm is the optimal polarized electric field for porous BNT-6BT ceramics. At this electric field, the porous piezoelectric constant d_{33} with pollen addition of 2.5 wt% reaches 131pC/N.

In order to fully polarize piezoelectric ceramics and give full play to good piezoelectric properties, it is necessary to select not only the appropriate polarization electric field intensity E, but also the appropriate polarization temperature. Therefore, the effect of polarization temperature on the piezoelectric performance of porous BNT-6BT ceramics was studied under the conditions of 30 min polarization time, 15 min pressure keeping and 5 kV/mm polarized electric field. The change pattern of the longitudinal piezoelectric coefficient d_{33} of 2.5% and 15% porous ceramics along with the polarization temperature T is shown in Fig. 5g. As the polarization temperature T increases, the longitudinal piezoelectric coefficient d_{33} increases. But when the polarization temperature reaches 90 °C, d_{33} remains basically unchanged. At lower temperatures, with the increase of temperature, the crystal axis ratio (c/a) becomes smaller, the domain activity increases, the resistance to domain transformation becomes smaller, and the domains are easy to be oriented, so the polarization is easier. When the polarization temperature T reaches 90 °C, most domains complete the transition, so the value of d_{33} does not change. This shows that the appropriate high-temperature polarization process is beneficial to weaken the pinning effect of the internal stress around the pore, promote the migration and rotation of the domain wall, and then improve the polarization efficiency.

4 Conclusion

Porous BNT-6BT ceramics with a porosity level of up to 43.6% were prepared with kiwi pollen as a template, and the influence mechanism of micropores on the dielectric and piezoelectric properties was analyzed by comparison with dense ceramics. U-shaped micropores ranging from 5 to 20 μm were formed inside the ceramic after burning the template. The ceramic protrusions offer barriers in the U-shaped micropores, which divide the pores into two interconnected regions. In the dense region, the grain size of 5% ceramics is in the range of about 1.5 μm, and with the increase of pollen addition, it decreases to

about 1 μm. With the increase of the amount of pollen added, the temperature stability of the dielectric constant of porous BNT-6BT ceramics increases significantly. The dielectric constant of porous ceramics decreases rapidly, then remains stable. The dielectric constant ε_{max} remains above 1500. The piezoelectric data indicates that the longitudinal piezoelectric coefficient d_{33} and the transverse piezoelectric coefficient d_{31} of the porous BNT-6BT ceramics decrease gradually, but they are better maintained. This is due to the fact that the ceramic barrier in the U-shaped micropores hinders the pinning effect of the micro stress and strain on the domain wall. When the polarized electric field strength E is 6 kV/mm and the polarization temperature T is 90 °C, the porosity of 2.5% ceramics reaches 10.3% and the piezoelectric constant d_{33} reaches 131pC/N. The study also shows that the appropriate high-temperature polarization process is beneficial to weaken the pinning effect of the internal stress around the pore, promote the migration and rotation of the domain wall, and then improve the polarization efficiency. Therefore, this work provides a deeper understanding of the impact of U-shaped micropores on the dielectric and piezoelectric properties of BNT-based ceramics, and provides reference for the application of porous BNT-based ceramics in piezoelectric energy conversion.

Acknowledgements

Author contributions

TL contributed to data curation, methodology, writing of the original draft, and visualization. HD contributed to ensure that the descriptions are accurate and agreed by all authors. NK and HL contributed to investigation and formal analysis. SX and ZL contributed to supervision, writing, and reviewing of the manuscript. XD participated in the writing, review and editing of the manuscript.

Funding

Data availability

The data supporting the findings of this study are available within the article. All data generated and analyzed during this study are included in this article.

Declarations

Conflict of interest The authors declare that they have no known competing financial interests or personal relationships that could have appeared to influence the work reported in this paper.

References

1. A. Ignatiev, Y.Q. Xu, N.J. Wu et al., Mater. Sci. Eng. B. **56**, 191–194 (1998). https://doi.org/10.1016/S0921-5107(98)00220-7

2. D. Bochenek, Z. Surowiak, S.V. Gavrilyachenko et al., Arch. Acoust. **30**, 87–107 (2005). https://doi.org/10.1091/CC-82-0475

3. C.Y. Ma, H.L. Du, J. Liu et al., Ceram. Int. **48**, 5428–5433 (2022). https://doi.org/10.1016/j.ceramint.2021.11.086

4. H.P. Ran, H.L. Du, C.Y. Ma et al., Sci. Adv. Mater. **13**, 741–747 (2021). https://doi.org/10.1166/sam.2021.3943

5. H.L. Du, C.Y. Ma, W.L. Ma et al., Process. Appl. Ceram. **12**, 303–312 (2018). https://doi.org/10.2298/PAC1804303D

6. R. Dittmer, W. Jo, J. Rödel et al., Adv. Funct. Mater. **22**, 4208–4215 (2012). https://doi.org/10.1002/adfm.201200592

7. L. Wu, X. Shi, H.L. Du et al., AIP Adv. **11**, 055305 (2021). https://doi.org/10.1063/5.0049923

8. S.T. Zhang, A.B. Kounga, E. Aulbach et al., Appl. Phys. Lett. **91**, 112906 (2007). https://doi.org/10.1063/1.2783200

9. K. Maeda, I. Fujii, K. Nakashima et al., J. Ceram. Soc. Jpn. **121**, 698–701 (2013). https://doi.org/10.2109/jcersj2.121.698

10. D.A. Giannakoudakis, M. Barczak, F. Pearsall et al., Chem. Eng. J. **384**, 123280 (2020). https://doi.org/10.1016/j.cej.2019.123280

11. D. N. Feng, H. L. Du, H. P. Ran, et al., J. Solid. State. Chem. 310, 123081 (2022). https://doi.org/10.1016/j.jssc.2022.123081

12. R. Stanculescu, C.E. Ciomaga, L. Padurariu et al., J. Alloys Compd. **643**, 79–87 (2015). https://doi.org/10.1016/j.jallcom.2015.03.252

13. F. Gheorghiu, L. Padurariu, M. Airimioaei et al., J. Am. Ceram. Soc. **100**, 647–658 (2017). https://doi.org/10.1111/jace.14587

14. H. Xu, H.L. Du, L. Kang et al., J. Renew. Mater. **9**, 2129 (2021). https://doi.org/10.32604/jrm.2021.016090

15. J. Roscow, Y. Zhang, J. Taylor, C.R. Bowen, Eur. Phys. J. Spec. Top. **224**, 2949–2966 (2015). https://doi.org/10.1140/epjst/e2015-02600-y

16. J.I. Roscow, R.W.C. Lewis, J. Taylor, C.R. Bowen, Acta Mater. **128**, 207–217 (2017). https://doi.org/10.1016/j.actamat.2017.02.029

17. S.L. Jiang, P. Liu, X.S. Zhang et al., J. Alloys Compd. **636**, 93–96 (2015). https://doi.org/10.1016/j.jallcom.2015.02.153

18. K.S. Srikanth, V.P. Singh, R. Vaish, J. Eur. Ceram. Soc. **37**, 3943–3950 (2017). https://doi.org/10.1016/j.jeurceramsoc.2017.05.015

19. D. Piazza, C. Galassi, A. Barzegar, D. Damjanovic, J. Electroceram. **24**, 170–176 (2010). https://doi.org/10.1007/s10832-008-9553-8

20. Y. Zhang, J. Roscow, M.Y. Xie, C. Bowen, J. Eur. Ceram. Soc. **38**, 4203–4211 (2018). https://doi.org/10.1016/j.jeurceramsoc.2018.04.067

21. R. Khachaturyan, S. Zhukov, J. Schultheiß et al., J. Phys. D **50**, 045303 (2016). https://doi.org/10.1088/1361-6463/aa519c

22. C. Padurariu, L. Padurariu, L. Curecheriu et al., Ceram. Int. **43**, 5767–5773 (2017). https://doi.org/10.1016/j.ceramint.2017.01.123

23. E.W. Yap, J. Glaum, J. Oddershede, J.E. Daniels, Scr. Mater. **145**, 122–125 (2018). https://doi.org/10.1016/j.scriptamat.2017.10.022

24. T.T. Xu, C.A. Wang, J. Eur. Ceram. Soc. **36**, 2647–2652 (2016). https://doi.org/10.1016/j.jeurceramsoc.2016.03.032

25. T. Ohji, M. Fukushima, Int. Mater. Rev. **57**, 115–131 (2012). https://doi.org/10.1179/1743280411Y.0000000006

26. P. Colombo, E. Bernardo, L. Biasetto, J. Am. Ceram. Soc. **87**, 152–154 (2004). https://doi.org/10.1111/j.1551-2916.2004.00152.x

27. L. Biasetto, P. Colombo, M.D.M. Innocentini, S. Mullens, Ind. Eng. Chem. Res. **46**, 3366–3372 (2007). https://doi.org/10.1021/ie061335d

28. A. Ando, M. Kamikura, Y. Takeoka et al., Sci. Technol. Adv. Mater. **22**, 511–521 (2021). https://doi.org/10.1080/14686996.2021.1936628

29. M. Descamps, O. Richart, P. Hardouin et al., Ceram. Int. **34**, 1131–1137 (2008). https://doi.org/10.1016/j.ceramint.2007.01.004

30. J.J. Wang, J. Wei, Int. J. Biol. Macromol. **176**, 558–566 (2021). https://doi.org/10.1016/j.ijbiomac.2021.02.106

31. W.F. Zhou, H.L. Du, L. Kang et al., Materials. **15**, 1130 (2021). https://doi.org/10.3390/ma15031130

32. B. Beal, A. Selby, C. Atwater et al., Environ. Prog. Sustain. **38**, 13150 (2019). https://doi.org/10.1002/ep.13150

33. Q. Jing, X.J. Li, Acta Phys. Sin. **68**, 057701 (2019). https://doi.org/10.7498/aps.68.20181790

34. F.L. Min, X.Y. Wang, M.D. Li, Y.X. Ni, J. Mater. Civ. Eng. **33**, 04020502 (2021). https://doi.org/10.1061/(ASCE)MT.1943-5533.0003552

35. T.T. Dele-Afolabi, M.A. Azmah Hanim, O.J. Ojo-Kupoluyi et al., Int. J. Appl. Ceram. Technol. **18**, 244–252 (2021)

36. Y.W. Kim, S.H. Kim, H.D. Kim et al., J. Mater. Sci. **39**, 5647–5652 (2004). https://doi.org/10.1023/B:JMSC.0000040071.55240.85

37. N. Ma, B.P. Zhang, W.G. Yang, D. Guo, J. Eur. Ceram. Soc. **32**, 1059–1066 (2012). https://doi.org/10.1016/j.jeurceramsoc.2011.11.014

38. V.A. Lukacs, R. Stanculescu, L. Curecheriu et al., Ceram. Int. **46**, 523–530 (2020). https://doi.org/10.1016/j.ceramint.2019.08.292

39. Q.M. Zhang, W. Cao, H. Wang et al., J. Appl. Phys. **73**, 1403–1410 (1993). https://doi.org/10.1063/1.353261

40. A.C. Hladky-Hennion, J.N. Decarpigny, J. Acoust. Soc. Am. **94**, 621–635 (1993). https://doi.org/10.1121/1.406878

41. H. Banno, Ceram. Bull. **66**, 1332–1337 (1987). https://doi.org/10.7567/jjaps.26s2.50

42. D. Damjanovic, Rep. Prog. Phys. **61**, 1267 (1998). https://doi.org/10.1088/0034-4885/61/9/002

43. J. Qi, L. Xiao-Juan, Acta. Phys. Sin-Ch. Ed. **68**, 057701 (2019). https://doi.org/10.7498/aps.68.20181790

44. M.M. Carroll, A.C. Holt, J. Appl. Phys. **43**, 1626–1636 (1976). https://doi.org/10.1063/1.1661372